

AD-A071 339

HARRY DIAMOND LABS ADELPHI MD
DESIGN STUDY FOR AN AURORA MODIFICATION LEADING TO A 100-TERAWA--ETC(U)
FEB 79 A G STEWART, G A HUTTLIN

F/G 20/3

UNCLASSIFIED

HDL-TM-79-3

NL

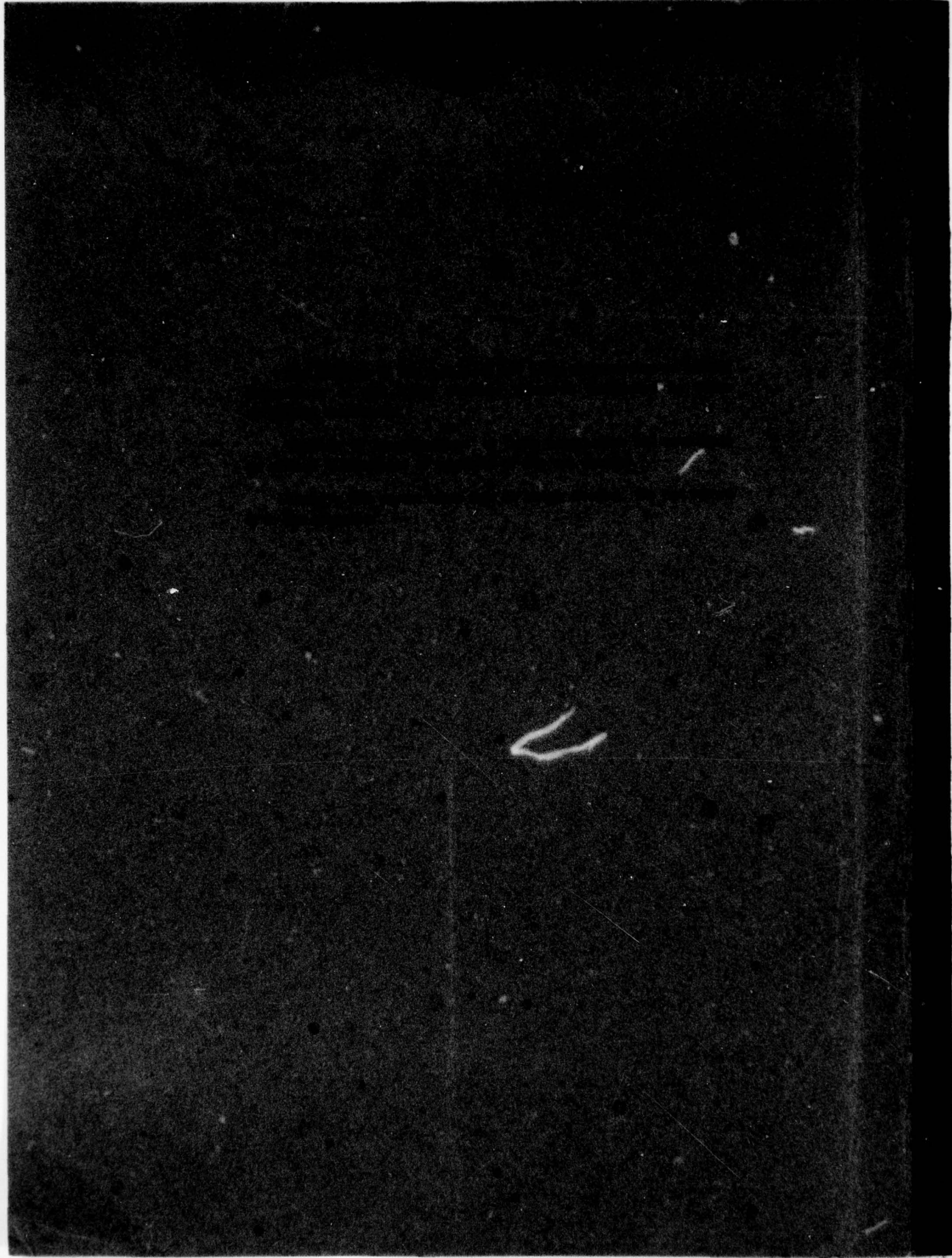
1 OF
AD
A071339



END
DATE
FILMED
8 --79
DDC

ADA071339

39 01 18 000



UNCLASSIFIED

SECURITY CLASSIFICATION OF THIS PAGE (When Data Entered)

14) REPORT DOCUMENTATION PAGE		READ INSTRUCTIONS BEFORE COMPLETING FORM
1. REPORT NUMBER HDL-TM-79-3	2. GOVT ACCESSION NO.	3. RECIPIENT'S CATALOG NUMBER
4. TITLE (and Subtitle) Design Study for an AURORA Modification Leading to a 100-Terawatt Nuclear Weapon Radiation Simulator		5. TYPE OF REPORT & PERIOD COVERED Technical Memorandum
6. AUTHOR(s) Alexander G. Stewart George A. Huttlin		7. CONTRACT OR GRANT NUMBER(s)
8. PERFORMING ORGANIZATION NAME AND ADDRESS Harry Diamond Laboratories 2800 Powder Mill Road Adelphi, MD 20783		10. PROGRAM ELEMENT, PROJECT, TASK AREA & WORK UNIT NUMBERS Program Ele: 6.27.10.H
11. CONTROLLING OFFICE NAME AND ADDRESS Director Defense Nuclear Agency Washington, DC 20305		12. REPORT DATE February 1979
13. MONITORING AGENCY NAME & ADDRESS (if different from Controlling Office) 12) 22p.		14. NUMBER OF PAGES 20
15. SECURITY CLASS. (of this report) UNCLASSIFIED		
16. DISTRIBUTION STATEMENT (of this Report) Approved for public release; distribution unlimited.		
17. DISTRIBUTION STATEMENT (of the abstract entered in Block 20, if different from Report) 16) G37IAXY X970		
18. SUPPLEMENTARY NOTES HDL Project: 201721 DRCMS Code: 36AA.7100.62710 This work was sponsored by the Defense Nuclear Agency under subtask G37IAXYX970 AURORA, work unit 07.		
19. KEY WORDS (Continue on reverse side if necessary and identify by block number) High pulsed power High-intensity electron beams Accelerator technology		
20. ABSTRACT (Continue on reverse side if necessary and identify by block number) The AURORA machine can be converted to provide beam power outputs near the 10^{14} -W power level into low impedance loads. The proposed conversion is based on a novel approach to pulse power intensification. The approach can be adapted to AURORA in differing configurations. A device of toroidal geometry utilizes the fast pulse charge capability of the AURORA generator to inject a traveling electromagnetic wave into a toroidal oil-filled coaxial line. From the point of injection, electromagnetic waves are propagated along the axis of the torus in opposite directions and at some time t will		

DD FORM 1 JAN 73 1473 EDITION OF 1 NOV 65 IS OBSOLETE

UNCLASSIFIED

SECURITY CLASSIFICATION OF THIS PAGE (When Data Entered)

1

10 to the 14th power

163 050

LB

→ next page

UNCLASSIFIED

SECURITY CLASSIFICATION OF THIS PAGE(When Data Entered)

meet each other at the end of the torus diametrically opposite the injection point. As the electromagnetic waves overlap, that portion of their energy stored in the magnetic field will be transformed into electrostatic energy, and the voltage in this region will double. At some optimum preselected time t^* , where $t^* > t$, the toroidal line is then switched circumferentially into an oil-insulated three-electrode parallel-plate transmission line to the diode load. A transmission-line model for the complete system has been developed and analyzed by computer to determine energy transfer efficiencies and power inputs into a matched ohmic load. It has been determined that peak power levels of 90 TW are achievable in a pulse of 30 ns full width at half maximum.

Accession For	
NTIS GRA&I	<input checked="" type="checkbox"/>
DDC TAB	<input type="checkbox"/>
Unannounced	<input type="checkbox"/>
Justification	<input type="checkbox"/>
By _____	
Distribution/ _____	
Availability Codes	
Dist.	Avail and/or ex special
A	

UNCLASSIFIED

SECURITY CLASSIFICATION OF THIS PAGE(When Data Entered)

CONTENTS

	Page
1. INTRODUCTION	5
2. PRINCIPLE OF PULSE COMPRESSION AND IMPEDANCE TRANSFORMATION	5
2.1 Application to Geometries Consisting of Right-Angled Coaxial Cylinders Discharging into Triangular Strip Feed Lines.....	5
2.2 Application to Toroidal Geometries	6
2.2.1 Single-Ended Pulse Injection	6
2.2.2 Double-Ended Pulse Injection	7
3. LINES IN CASCADE	7
3.1 Combination of Straight Coaxial Cylinders with Torus	7
3.2 Combination of Straight Coaxial-Cylinder Geometries	8
4. DETAILED ANALYSIS OF TOROIDAL GEOMETRY FRONT-END CONVERSION TO AURORA	8
4.1 Combination of Existing Vacuum Coaxial Lines into Single Coaxial Line.....	8
4.2 Design Considerations for Torus.....	9
4.2.1 Torus Dimensions and Determination of Input and Output Impedances.....	9
4.2.2 Transmission-Line Analysis	10
4.2.3 Electric Fields in Torus	10
4.3 Torus Switch Discharge Characteristics	12
4.4 Design of Strip Wedge Transformer.....	12
4.5 Prepulse Estimates and Effects	13
4.6 Analysis of Discharge Phase of Torus	14
4.7 Field Emission Diode Design	16
5. CONCLUSIONS	16
DISTRIBUTION	17

FIGURES

1 Discharge of pulse-charged longitudinal line into strip feed line	6
2 Pulse injection into torus	7
3 Use of low impedance converter modules as torus pulse charge injector.....	7
4 Pulse charging half torus from triangular strip feed line	8
5 Pulse compression by using three-stage series-connected straight coaxial geometries.....	8

FIGURES (Cont'd)

	Page
6 Junction of AURORA coaxial lines into single coaxial line	9
7 Low impedance converter	9
8 Transmission-line model for charge phase.....	10
9 Overlapping voltage pulses in torus	10
10 Voltage profile in torus for 12-MV blumlein charging at time = 350 ns.....	11
11 Statistical area for breakdown in torus	11
12 Center electrode of wedge transformer	13
13 Representative circuit for discharge phase of torus	15
14 Diode voltage: blumlein stores charged to -12 MV and torus switched at 350 ns	15
15 Diode current: blumlein stores charged to -12 MV and torus switched at 350 ns	15
16 Power delivered to diode: blumlein stores charged to -12 MV and torus switched at 350 ns. 15	15
17 Low impedance diode	16

1. INTRODUCTION

The effectiveness of strategic weapons systems depends on their ability to function in a hostile nuclear environment. For some years now, there has been a shift of emphasis away from systems hardening through underground testing toward laboratory testing in specially equipped simulation centers. These centers employ a variety of pulsed-power sources for the production of intense electron beams, electromagnetic waves, and gamma and neutron pulses. While these test facilities have proved invaluable in simulating certain aspects of a warhead's radiation output, there remains a need for a source more closely approximating the outputs of real weapons. One such source could be the radiation emanating from a highly compressed pellet. Recent studies¹ have shown that a relativistic electron beam with peak powers of 10^{14} to 10^{15} W would be required for this purpose, or, alternatively, ion beams at 10^{12} to 10^{13} W could accomplish this same goal. Techniques for the efficient conversion of relativistic electron beams to focused ion beams have been investigated by Humphries² and Verdeyen.³ Electron-to-ion conversion efficiencies as high as 50 percent have been reported.

One limitation to the extraction of very intense power pulses from the Harry Diamond Laboratories AURORA generator⁴ in its present form is the rather long discharge time of the blumleins. A second disadvantage is the high internal impedance of these lines (21Ω), which makes them inefficient for energy transfer to low impedance loads. Studies conducted for the

present AURORA Modification Project have shown that it is possible to use the AURORA Marx generator to charge a water-insulated pulse-forming network (PFN) to generate 20 TW. This approach, however, does not seem capable of extension to significantly higher power outputs. The purpose of this study is to demonstrate that it may be possible to extract power outputs closer to the 100-TW level and to operate efficiently into loads near 1Ω .

2. PRINCIPLE OF PULSE COMPRESSION AND IMPEDANCE TRANSFORMATION

The principle of operation of the device is described in detail⁵ in U.S. Patent 4,003,007, so only the basic ideas are discussed here.

2.1 Application to Geometries Consisting of Right-Angled Coaxial Cylinders Discharging into Triangular Strip Feed Lines

Referring to figure 1, a pulse of duration T_0 is injected into the left-hand side of the center conductor of the coaxial-cylinder element referred to as the longitudinal line. As generally assumed, when the pulse is transmitted into the line and then reflected from the open-circuit end of the line, the line is statically charged all along its length. It is also generally assumed that the length of this line is very much larger than its diameter. A second line, identified as the triangular strip feed line, is attached to the longitudinal line as shown in figure 1. The center conductor of the feed line is separated from the center conductor of the longitudinal line so that, during the charging phase of the latter, the former remains near ground potential. Since the right-hand side of the longitudinal line is an open circuit, the in-

¹M. J. Clauser and M. A. Sweeney, *Charged-Particle Beam Implosion of Fusion Targets*, International Topical Conference on Electron Beam Fusion, Albuquerque, NM (November 1975).

²S. Humphries, J. J. Lee, and R. N. Sudan, *Generation of Intense Pulsed Ion Beams*, *Appl. Phys. Lett.*, 25 (1974) 20.

³J. T. Verdeyen, D. A. Swanson, B. E. Cherrington, and W. L. Johnson, *The Use of Electronic Space Charge to Accelerate, Focus and Bunch Ions for Pellet Compression*, *Appl. Phys. Lett.*, 27 (October 1975).

⁴B. Bernstein and I. Smith, *Aurora, an Electron Accelerator*, *IEEE Trans. Nucl. Sci.*, 20 (June 1973), 294.

⁵A. G. Stewart, *High Power Pulse Compression Techniques*, U.S. Patent 4,003,007 (11 January 1977).

jected pulse is reflected on arrival at this end, and the reversal doubles the amplitude of the incident pulse. This reflected pulse then is propagated back toward the point of origin. The voltage developed across the gap spacing between the two center conductors also is doubled. When the reflected wave has completed approximately two thirds of its travel toward the injection point, a controlled electrical breakdown between the two inner electrodes is initiated at the extreme right-hand side of the system. The propagation of this breakdown (switching) is such that, when the reflected wave finally reaches the point of injection, breakdown also is occurring at this time and place.

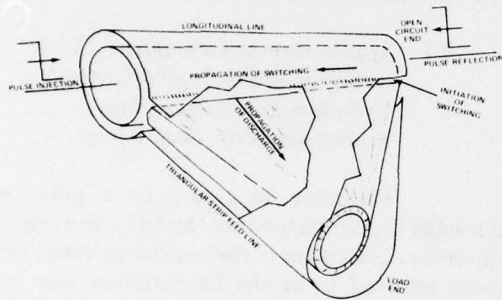


Figure 1. Discharge of pulse-charged longitudinal line into strip feed line.

The triangular shape of the strip feed line promotes the synchronous arrival of the discharge pulse at the output end of this line. This output end, known as the load end, is shown in coaxial geometry, but this is a convenience and is not necessary in principle.

The discharge pulse is of shorter duration than the injected pulse by the factor $(2\pi r)/(2L)$, where L is the length of the longitudinal line and r is its mean radius. This ratio assumes that switch effects can be ignored and also that there is no pulse spreading with propagation of the discharge to the load.

The input impedance, Z_i , of the longitudinal line is given by the relationship

$$Z_i = \frac{60}{\sqrt{K}} \ln \frac{b}{a} \text{ } (\Omega) ,$$

where K is the dielectric constant of the medium between the coaxial cylinders and a and b are the inner and outer radii, respectively. The discharge impedance, Z_o , of this line is, however, governed by the equation appropriate to a triplanar strip line, that is,

$$Z_o = \frac{1}{2} \cdot \frac{377}{\sqrt{K}} \cdot \frac{b - a}{L} \text{ } (\Omega) . \quad (1)$$

Since Z_o can be readily made to be significantly lower than Z_i , this technique of energy extraction is capable also of impedance transforming with very high efficiencies.

The impedance of the strip feed line can be readily matched to the discharge impedance of the longitudinal line.

2.2 Application to Toroidal Geometries

A second application is to inject the pulse into a toroidal geometry. Toroidal geometries have the advantage that they can be made more compact than the equivalent straight coaxial-cylinder approach. Also, the switching requirements are less stringent since all the switches are operated synchronously, rather than in a controlled rate of breakdown. Finally, the symmetry of the discharge line is less likely to lead to pulse spreading as the energy is propagated toward the load.

2.2.1 Single-Ended Pulse Injection

The single-ended toroidal pulse injection is illustrated in figure 2. Traveling waves are propagated around both arms of the torus, and their leading edges are allowed to

overlap until the voltage reaches approximately one half of the peak amplitude before synchronous triggering is induced along the inside perimeter of the torus. The output line from the torus is shown in figure 2 configured in cylindrical geometry, which would make it compatible for matching to the type of diode structures which have been developed for other systems, that is, Blackjack and Python.* The discharge line need not be directed inward toward the axis of the torus. It could, with equal effectiveness, be directed outward (at 180 deg) away from the torus axis.

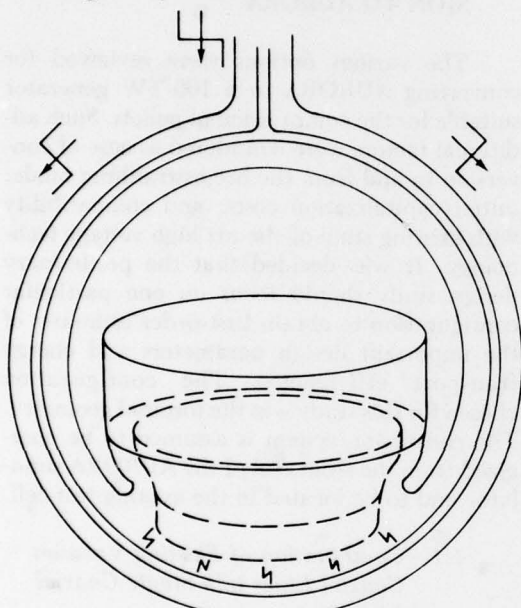


Figure 2. Pulse injection into torus.

2.2.2 Double-Ended Pulse Injection

Several studies have been made on the design of a low impedance conversion of AURORA charged directly from the AURORA Marx generator. The major design efforts in these studies were directed toward a two-module output device. As shown in figure 3, it is conceptually feasible to use each of these

*Machines developed by Maxwell Laboratories and Physics International, respectively.

modules as the pulse injectors into each of the two arms of a half torus and to extract the energy from this half torus in the same manner as described in section 2.2.1. This approach has an additional advantage in that the pulse injection time is very short (~ 60 ns), which would permit higher fields and, hence, smaller torus dimensions, for the same stored energy. This smaller torus would permit even shorter pulse outputs.

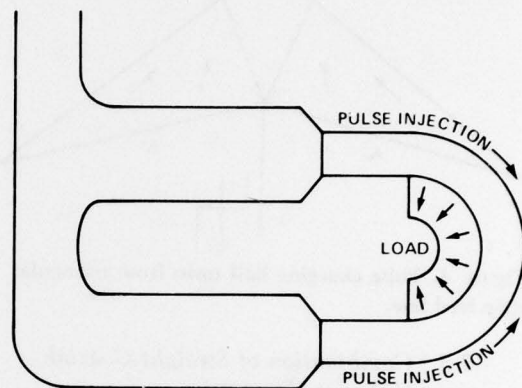


Figure 3. Use of low impedance converter modules as torus pulse charge injector.

3. LINES IN CASCADE

There are distinct advantages to be gained from making the pulse injection time as short as possible, especially if high-energy, ultrashort (<20 ns) pulse outputs are desired. By employing two or more of the injection devices in tandem, this goal of <20 ns can be achieved.

3.1 Combination of Straight Coaxial Cylinders with Torus

In figure 4, the two longitudinal lines A and A', pulse-charged from a single-ended injection point, are discharged into the two arms of a half torus. Because the pulse duration at the output of the feed line is significantly shorter than the pulse duration at

the input, the dimensions of the half torus can be considerably smaller than are necessary if the initial pulse alone is used to charge the torus. The smaller the torus, the faster the energy that can be extracted from it and the lower the output impedance of the system.

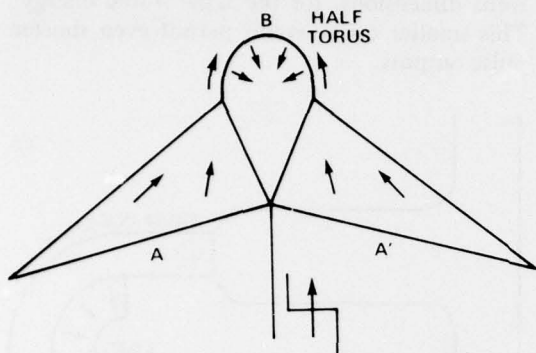


Figure 4. Pulse charging half torus from triangular strip feed line.

3.2 Combination of Straight Coaxial Cylinder Geometries

In figure 5, the output of the first feed line is used as input to a second longitudinal line, which is similarly charged

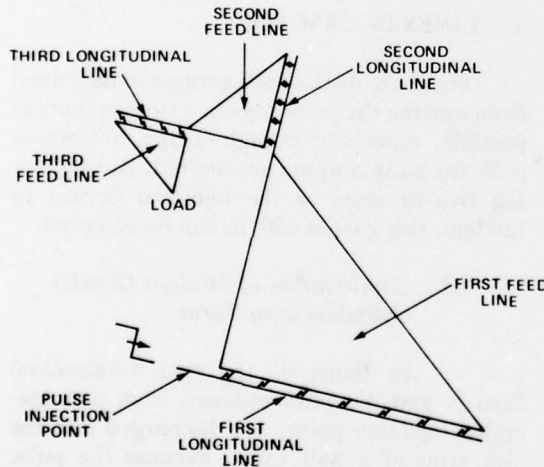


Figure 5. Pulse compression by using three-stage series-connected straight coaxial geometries.

and discharged as the first element, but whose overall dimensions are smaller because of the higher permissible electric-field gradients. Further additions can be made, as shown in figure 5, each stage leading in principle to pulse outputs of shorter duration, lower impedance, and higher power.

4. DETAILED ANALYSIS OF TOROIDAL GEOMETRY FRONT-END CONVERSION TO AURORA

The various options were reviewed for converting AURORA to a 100-TW generator suitable for the compression of pellets. Such additional factors were considered as ease of conversion to and from the bremsstrahlung mode, initial capitalization costs, and compatibility with existing state-of-the-art high voltage technology. It was decided that the preliminary design study should focus on one particular configuration to obtain first-order estimates of the important design parameters and energy transport efficiencies. The configuration chosen for this study was the toroidal geometry. The conversion system is assumed to be energized from the front end of the AURORA simulator and to be located in the existing test cell.

4.1 Combination of Existing Vacuum Coaxial Lines into Single Coaxial Line

The present AURORA simulator has four separate 50Ω vacuum coaxial lines feeding four separate field-emission diodes. It would be necessary for these to be filled with some suitable dielectric and, for simplicity, to be the same insulating medium as used in the torus itself—oil. (For short pulse output applications, transformer oil ($K = 2.3$) is preferred to water as an insulant because of the higher velocity of electromagnetic waves in oil.) Filling each of these coaxial lines with transformer oil without changing either the inner or the

outer radii of the coaxial cylinders would reduce their individual impedances to 33Ω . To achieve single-point pulse injection into the torus, it is necessary to combine this array of coaxial lines into a single coaxial line (fig. 6). The parallel impedance of the four coaxial lines is 8.24Ω , and, to eliminate reflections at the junction, the impedance of the single coaxial-line output should be matched to this value.

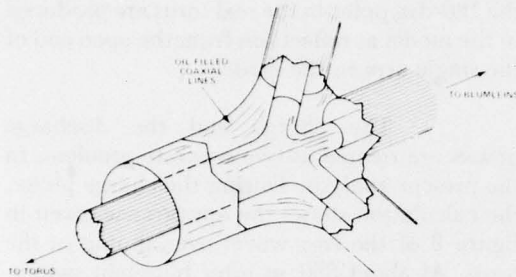


Figure 6. Junction of AURORA coaxial lines into single coaxial line.

4.2 Design Considerations for Torus

To arrive at a feasible conceptual design for the torus, many factors must be considered and analyzed for self-consistency and compatibility with the state of the art of high voltage technology. Principal among these are the dimensions of the torus that determine its input and output impedances and the electric fields experienced within it.

4.2.1 Torus Dimensions and Determination of Input and Output Impedances

The preliminary design chosen for detailed study in this report is shown in figure 7. The dimensions are those that were arrived at after consideration of the various constraints, such as available space in the AURORA test cell, energy transfer efficiencies, and electrical breakdown conditions. The final

dimensions of the preliminary study are presented here.

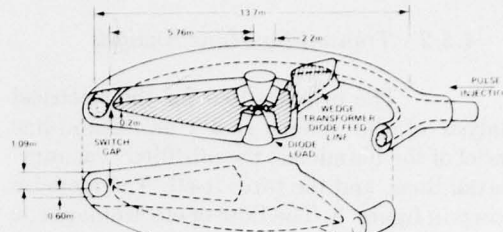


Figure 7. Low impedance converter.

The major diameter, D , of the torus is 13.7 m , and the coaxial cylinders have radii b and a of 0.1091 m and 0.600 m , respectively, giving a gap separation of 0.491 m . The line impedance, Z_0 , of the torus is therefore given by

$$Z_0 = (60/\sqrt{K}) \ln(b/a) = 23.7 \text{ } (\Omega)$$

For ideal matching to the pulse injection line, this impedance should be twice the impedance of the pulse injection line— 16.48Ω —so some energy is lost due to reflections at this interface. In fact, for ideal matching to the four parallel blumleins (overall $Z = 5 \Omega$), the torus impedance should be even lower (closer to 10Ω). This higher impedance torus, on the other hand, presents less stringent requirements on the fields to be sustained in the oil, and, since the intent of this preliminary study was to acquire only first-order design information, this trade-off was judged to be a reasonable one.

The output impedance of the torus is inversely proportional to the length of the element being discharged and, for this case, was chosen to be three quarters of the circumference— 270 deg . As will be shown, this gives a discharge impedance of 1.89Ω , which is not an optimum value in terms of basic design goals, but is sufficiently close to provide

valuable baseline data for development of the concept.

4.2.2 Transmission-Line Analysis

The primary tool for the electrical analysis of the system is a transmission-line model of the blumleins, the oil-filled "vacuum" coaxial lines, and the torus itself. The model is shown in figure 8. The flow of electromagnetic waves through the model was calculated with an expanded form of a computer code supplied by J. Shipman of the Naval Research Laboratory. Since it is assumed that each of the four blumlein subsystems is identical, the entire array of blumleins is represented in the model by elements of one blumlein, each element having one fourth the impedance of the corresponding element in the actual blumlein.

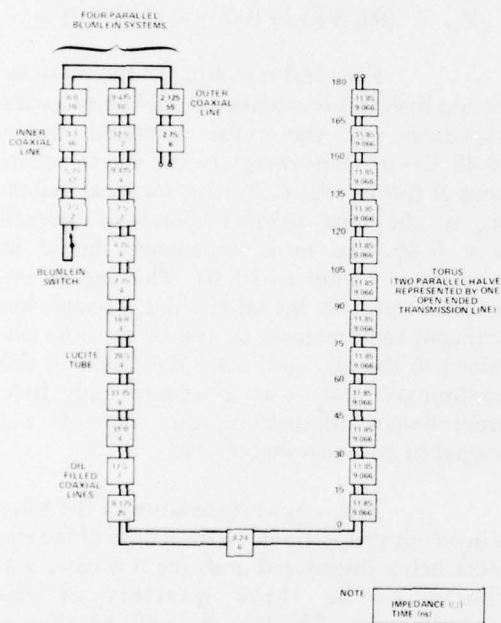


Figure 8. Transmission-line model for charge phase

A similar simplification is done for the torus. In actuality, a single oil coaxial line divides the torus into the two arms, one

directed to the left, the other directed to the right. At 180 deg from the torus entry point, these arms join. Because what is happening in the left arm of the torus is assumed to be identical to what is happening in the right arm, the two arms can be replaced in the model by one arm having half the impedance of either actual arm and an identical one-way transmission time from 0 to 180 deg. Waves having passed the 180-deg point in the real torus are produced in the model as reflections from the open end of the single arm in the model.

The charge and the discharge phases are treated as two separate problems in the present analysis. During the charge phase, the calculation shows the appearance given in figure 9 of the two waves overlapping in the torus. At about 350 ns after blumlein switching, the waves in the torus overlap to form the net voltage profile shown in figure 10. At this time, the current throughout the torus is negligible, and almost all the energy is stored electrostatically. This is the time chosen for switching the torus into its discharge configuration.

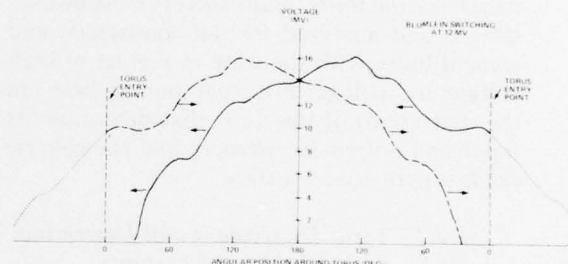


Figure 9. Overlapping voltage pulses in torus.

4.2.3 Electric Fields in Torus

At a given time and angular position in the torus, the maximum field, F , exists at the surface of the inner coaxial cylinder and is given by the relation

$$F = V_0 / [a \ln(b/a)] \quad ,$$

where V_0 is the voltage. The negative impulse breakdown strength for transformer oil is given approximately by the relation

$$F_- = 0.875A^{-0.07}t^{-0.333} \text{ (MV/cm)} ,$$

where F_- is the maximum permissible field, A is the area of the inner electrode in square centimeters, and t is the time in microseconds that the voltage exceeds 63 percent of its breakdown value. This equation is most readily applied in situations where a large area of an electrode is exposed uniformly to the same time-dependent field. This uniformity, however, is not the case in the torus as suggested by figures 9 and 10.

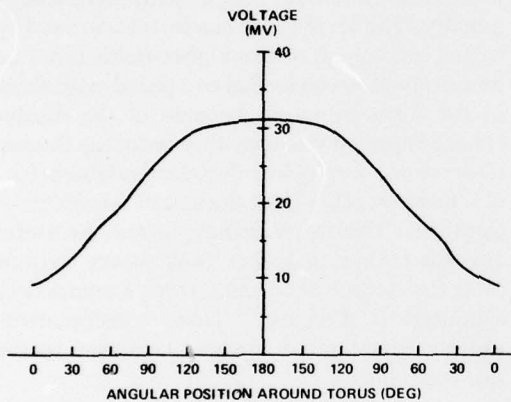


Figure 10. Voltage profile in torus for 12-MV blumlein charging at time = 350 ns.

To assess the ability of the torus to withstand breakdown, the function $V(t)$ was considered at each of 13 positions in the transmission-line model of the torus (every 15 deg from 0 through 180 deg). In using these functions $V(t)$, it was assumed that the torus would switch at 350 ns, thus drastically reducing the voltage within about 15 ns of the switching time. (Fifteen nanoseconds is the approximate transit time during the discharge

phase of the torus.) For argument, it was assumed that the maximum field given by a particular $V(t)$ was the breakdown field. These peak fields range from 0.47 to 0.90 MV/cm. The time parameters, t , were obtained from $V(t)$ and ranged from 0.065 to 0.185 us. Then, A was derived for each position by using the relations above.

Figure 11 relates A , as determined from the breakdown formula, to angular position in the torus. The horizontal axis is labeled also in terms of area measured along the center conductor. From this graph, the likelihood of an electric breakdown at any position in the torus is determined as follows:

Consider the voltage/time profile $V(t)$ at a given position in the torus. For this $V(t)$, A has been calculated (by use of the breakdown formula) over which $V(t)$ can be

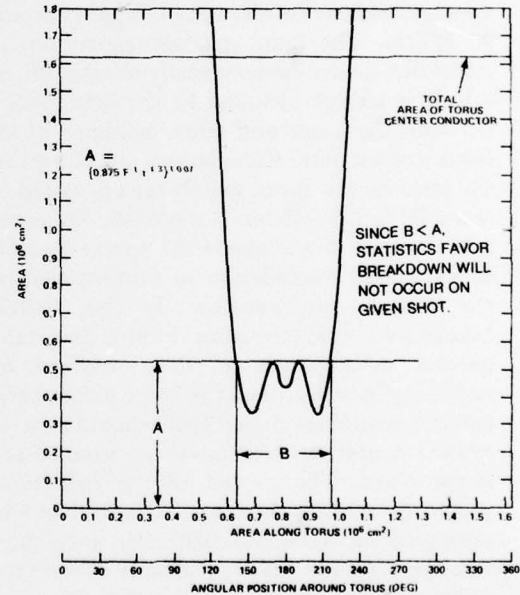


Figure 11. Statistical area for breakdown in torus.

sustained without breakdown. This A is compared with area B in the torus over which $V(t)$'s of the same or greater severity are experienced. If A is significantly greater than B , the spacing of the inner and outer conductors of the torus is adequate to prevent breakdown at the position under consideration.

As can be seen by looking over the entire torus, the design is favorable. For most positions, tolerable A is well in excess of the total area ($1.62 \times 10^6 \text{ cm}^2$) of the torus. From about 145 to 180 deg, however, the present design is only marginally adequate.

4.3 Torus Switch Discharge Characteristics

Experience on the AURORA simulator has shown that reproducible, multichannel switching in oil can be achieved by using positive-field enhanced-edge electrodes, for average fields in the main gap of approximately 25 MV/m. The main gap separation on the AURORA electrodes is typically about 0.46 m, which is almost identical to the gap spacing between the inner and outer cylinders of the torus studied here. Calculations also show that the field in the torus switch region would be about 50 to 100 MV/m. It is not known for certain whether this higher-field operation leads to an overall degradation or improvement of the switch performance. If the switch-breakdown characteristics follow the same general development as that observed for switching in water, then the faster pulse charge coupled with these higher fields should give improved operation with lower impedance and lower jitter. The overall switch inductance should be considerably smaller here than that estimated for AURORA (200 nH) since channels form around three quadrants of the torus perimeter, a distance of more than 30 m, as compared with the 3.7 m of edge of the AURORA midplane. These figures suggest an inductance of ~ 20 nH for the torus switch. This inductance is incorporated into the dis-

charge phase of the transmission-line calculation. No further development of this triggered switch concept has been undertaken in this study.

4.4 Design of Strip Wedge Transformer

The function of the strip wedge transformer is to transport the energy from the discharging torus to the diode. For maximum energy transport, the wedge impedance should be constant all along its discharge path, and, in the present study, this was the design criterion used. However, the wedge could be designed to transform the impedance from a relatively high impedance at the wedge input to a lower impedance at the wedge output with small energy penalty. The impedance can be transformed by taking advantage of the higher fields that can be sustained in the wedge compared with those in the torus primarily because of the shorter times of applied voltages, thus reducing the gap dimensions, and by locating the diode structure at a location other than the axis of symmetry of the torus. This latter technique may be useful also for obtaining higher peak power outputs than the output obtainable from a completely symmetrical discharge. These considerations are not investigated further, however, in the present report.

The impedance of the wedge may be shown to be approximately 2Ω as follows:

In its discharge phase following switchching, the torus behaves like an open-ended triplanar strip line with a plate spacing equal to the spacing between the inner and outer conductors of the torus, namely, $S = 0.491$ m. For this triplanar strip line, with an effective torus diameter $D = 13.7$ m and switching over 270 deg, the width W is $(270/360)\pi D = 32.3$ m. By use of equation (1), this gives an impedance of 1.89Ω for the triplanar strip line as formed by the torus itself.

The torus discharges into another triplanar strip line, the wedge transformer of

figure 7. Neglecting end effects, the impedance of the wedge remains constant for the wave front converging on the central load as long as the ratio S/W remains constant. That is, at smaller radii, proportionately smaller spacings are desired. At sufficiently small radii, this spacing results in fields in excess of breakdown conditions. However, as can be expected by looking at figure 12, the path of the wave front does not converge radially near the extremes of the discharge. This lack of convergence effectively increases $W(r)$, the length of the wave front at radius r , beyond the value for a strictly radial discharge. Now, considering end effects, the effect on $W(r)$ is further enhanced by the larger height of the central electrode (fig. 12) approaching the diode. The overall effect of the actual shape of the wedge transformer is to require that S decrease only by a factor of two instead of three to maintain the constant 1.89Ω impedance as the wave front approaches the diode. Alternatively, we could have Z increase by a factor of two instead of three as the wave front approaches the diode if we maintain a fixed S between the central electrode and the outer conductor.

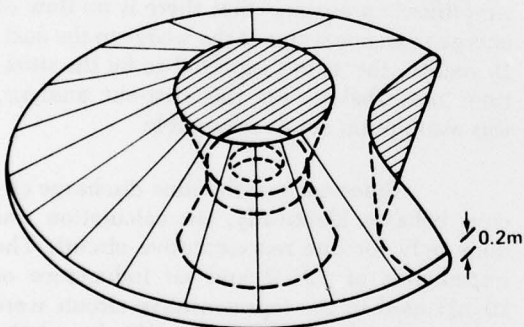


Figure 12. Center electrode of wedge transformer.

4.5 Prepulse Estimates and Effects

Because of capacitive coupling between that portion of the center conductor of the torus and the inner conductor of the strip line wedge transformer in the switch region, some fraction of the voltage impressed on the torus center conductor during the torus charge phase appears on the wedge transformer's inner conductor. This voltage in turn is transmitted to the diode cathode as a prepulse. Depending on the amplitude and the duration of this prepulse, the current emission and beam dynamics in the anode-cathode gap region can be significantly affected. Most of the information on prepulse has been empirically derived, and no comprehensive theory has been developed to predict its effects. It is known that large prepulses can induce premature pinching in the anode-cathode gap of high current diodes, and it is generally desirable to keep this voltage small. It is known also, however, that prepulse effects are sensitive to diode structure; that is, an identical prepulse injected into two dissimilar diode structures produces markedly different effects. Further, some workers have suggested that a well-controlled prepulse of small amplitude can even have beneficial effects on diode performance through preconditioning the cathode. It is not the intent of this study to make a comprehensive review of the literature to investigate these effects in detail, but rather to make an initial first-order calculation of the amplitude and the duration of the prepulse anticipated for the geometry chosen for this study.

When the geometry is considered as a parallel-plate capacitor, the capacitance, C_1 , between the inner conductor of the torus and

the inner conductor of the wedge transformer is, to a first approximation,

$$C_1 = K\epsilon_0 \frac{\text{area}}{\text{separation}}$$

$$= K\epsilon_0 \frac{2\pi r w f}{S} = 0.35 \text{ (nF)},$$

where

$$K = 2.3,$$

$$\epsilon_0 = 8.854 \text{ pF/m},$$

$f = 270/360$ deg, the fraction of the torus circumference of interest,

$r \approx 6.0$ m, the effective radius of curvature of the torus at this gap,

$w \approx 0.3$ m, the approximate width of the gap,

$S = 0.491$ m, the spacing of the inner conductor in the torus from the inner conductor of the wedge.

This value of C_1 is to be compared with the capacitance, C_2 , between the central conductor of the wedge transformer and the outer conductor (assumed to be at the constant $S = 0.491$ m),

$$C_2 = 2K\epsilon_0 \frac{f\pi(r_2^2 - r_1^2)}{S} = 5.5 \text{ (nF)},$$

where $r_2 = 5.76$, the outer radius of the wedge, and $r_1 = 2.2$ m, a reasonable value for the inner radius of the wedge. The factor of two accounts for both upper and lower gaps in the wedge transformer. Capacitances C_1 and C_2 appear in series dividing the voltage applied to the torus. This fact implies that the fraction

$$C_2^{-1}/(C_2^{-1} + C_1^{-1}) = 6 \text{ percent}$$

of the torus voltage appears as a prepulse.

This fraction could be smaller either if the spacing between the central wedge conductor and the outer conductor were to decrease at small radii or if the switch gap were to be increased.

4.6 Analysis of Discharge Phase of Torus

The discharge phase of the torus was treated as a problem separate from the charge phase. At the time (350 ns after blumlein switching) chosen for torus switching, the current throughout the torus was found to be negligible. At this time, almost all the energy is stored in the electric field, and this energy is distributed among the 12 transmission-line elements in the model. Since the torus switching has been restricted to 75 percent of the torus, only 9 of the 12 elements partake in the switching.

The discharge of each of the nine elements is handled by a separate circuit. This simplification assumes that there is no flow of energy from one sector of the wedge to the next. In reality, this is not expected to be the situation; nevertheless, for this first-cut analysis, this assumption seems reasonable.

Since each of the nine discharge circuits behaves identically, the calculation was done only for one representative circuit. The impedances of 1.8Ω and an inductance of 20 nH used in the representative circuit were scaled to apply to the entire 270 deg of the discharging torus and are shown in the circuit of figure 13. This analysis assumes that the impedance of the strip-line wedge is matched to that of the torus and is constant right up to the load. The one-way transit time of the element representing the torus is 13.04 ns and is the effective transit time given by

$$\frac{Z_{\text{discharge}}}{T_{\text{discharge}}} = \frac{Z_{\text{charge}}}{T_{\text{charge}}},$$

a condition that must be imposed so that the electrostatic energy of the torus in its charge configuration equals the electrostatic energy of the torus in its discharge configuration. Here Z_{charge} is 23.7Ω and T_{charge} is the transit time for 75 percent of the torus circumference ($T_{\text{charge}} = 81.5 \text{ ns}$).

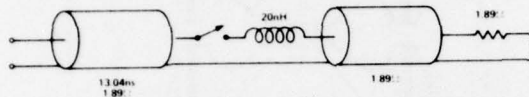


Figure 13. Representative circuit for discharge phase of torus.

In the representative calculation, a unit voltage was used for the initial voltage on the charged torus in its discharge configuration. The final scaling was later provided by normalizing to the appropriate average over the initial voltages on the nine segments of the torus model in its charge phase. The output voltage shown in figure 14 is scaled according to the average of the individual V_i , and the total current shown in figure 15 also is scaled according to the average of V_i . The power, however, scales according to the average of V_i^2 , and it is this scaling that is used in figure 16.

The effect of the prepulse was included in the calculation by imposing an initial voltage on the wedge equal to 6 percent of the unit voltage on the torus. In the calculation, it was assumed that the distribution of the prepulse throughout the wedge corresponds exactly with that of the voltage on the torus, which is not expected in actuality. Nevertheless, the trend of the effect is approximately accounted for and, since the effect of the prepulse on the overall pulse shapes is small anyway, this assumption causes no concern.

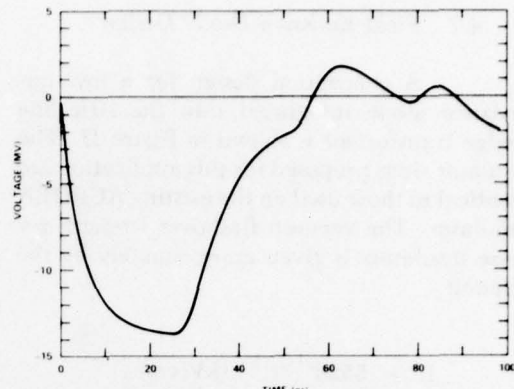


Figure 14. Diode voltage: blumlein stores charged to -12 MV and torus switched at 350 ns.

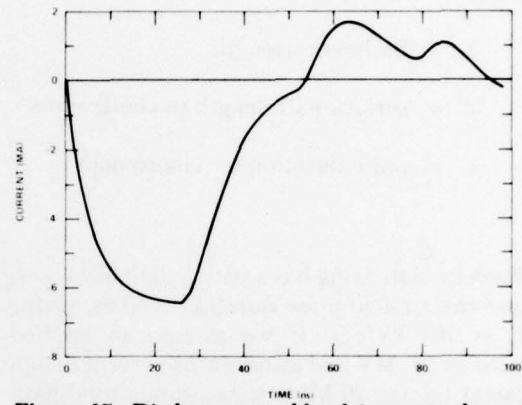


Figure 15. Diode current: blumlein stores charged to -12 MV and torus switched at 350 ns.

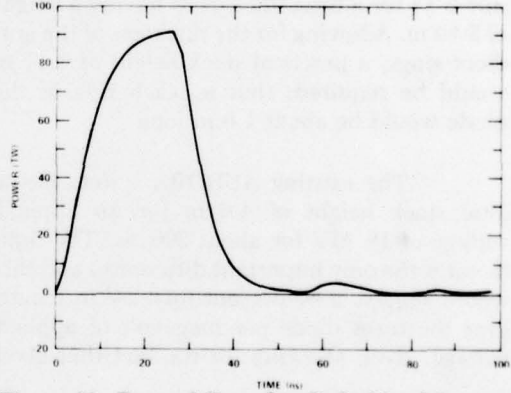


Figure 16. Power delivered to diode: blumlein stores charged to -12 MV and torus switched at 350 ns.

4.7 Field Emission Diode Design

A conceptual design for a low impedance diode integrated into the strip-line wedge transformer is shown in figure 17. The insulator rings proposed for this application are identical to those used on the existing AURORA simulator. The vacuum flashover strength for these insulators is given approximately by the relation

$$E = 552d^{-1/6}t^{-1/3} \text{ (kV/cm)},$$

where

E = flashover strength,

d = surface path length in centimeters,

t = pulse duration in nanoseconds.

Each insulator ring has a path length of 14 cm, and the applied pulse duration is 40 ns, giving $E = 104$ kV/cm. If we assume an applied pulse of 14 MV and assume a 70-percent design factor (giving 20 MV), we require a total path length of 20 MV/104 (kV/cm)—that is, 192 cm. Hence, the total number of rings required per side is 14 for a total stack of 28 having a height of 2.84 m. Allowing for the thickness of the gradient rings, a practical stack height of 3.11 m would be required; that is, each side of the diode would be about 1.6 m long.

The existing AURORA system has a total stack height of 4.6 m for an applied voltage of 18 MV for about 200 ns. The time factor is the only important difference, and this would suggest a 60-percent increase in length over the torus diode per megavolt of applied voltage. Even allowing for the fact that good

uniform field grading is more difficult for larger stack lengths, this increase still suggests that the torus diode may be marginally designed in terms of voltage hold-off capability. Lengthening the stack, however, does not present any obvious difficulties, and, lacking further corroborating data, we continue to assume that the proposed 3.1-m stack height is adequate for this study.

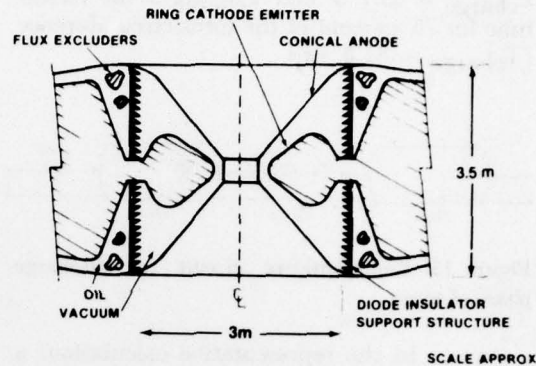


Figure 17. Low impedance diode.

5. CONCLUSIONS

A novel approach has been conceived for the production of short duration, ultrahigh power pulses into low impedance loads. The concept has been shown to be extremely versatile and can be adapted to AURORA in a wide variety of configurations. A selected toroidal geometry has been investigated, and analysis has shown that power outputs approaching 10^{14} W can be delivered to a low impedance load (1.89Ω) in 30 ns full width at half maximum. Further manipulation of the design should give a factor of two increase over these power output levels. With the exception of the diode, all of the design criteria are known to be compatible with the existing state of the art of high voltage pulsed-power technology.

DISTRIBUTION

DEFENSE DOCUMENTATION CENTER
CAMERON STATION, BUILDING 5
ALEXANDRIA, VA 22314
ATTN DDC-TCA (12 COPIES)

COMMANDER
USA RSCH & STD GP (EUR)
BOX 65
FPO NEW YORK 09510
ATTN LTC JAMES M. KENNEDY, JR.
CHIEF, PHYSICS & MATH BRANCH

COMMANDER
US ARMY MATERIEL DEVELOPMENT &
READINESS COMMAND
5001 EISENHOWER AVENUE
ALEXANDRIA, VA 22333
ATTN DRXAM-TL, HQ TECH LIBRARY

COMMANDER
USA MISSILE & MUNITIONS CENTER
& SCHOOL
REDSTONE ARSENAL, AL 35809
ATTN ATSK-CTD-F

COMMANDER
US ARMY ARMAMENT MATERIEL
READINESS COMMAND
ROCK ISLAND, IL 61299
ATTN DRSTAR-LEP-L, TECHNICAL LIBRARY

DIRECTOR
US ARMY BALLISTIC RESEARCH LABORATORY
ABERDEEN PROVING GROUND, MD 21005
ATTN DRDAR-TSB-S (STINFO)

DIRECTOR
US ARMY MATERIEL SYSTEMS
ANALYSIS ACTIVITY
ABERDEEN PROVING GROUND, MD 21005
ATTN DRXSY-MP

ASSISTANT TO THE SECRETARY OF DEFENSE
ATOMIC ENERGY
DEPARTMENT OF DEFENSE
WASHINGTON, DC 20301
ATTN ATSD (AE)

DIRECTOR
DEFENSE ADVANCED RESEARCH
PROJECTS AGENCY
ARCHITECT BLDG
1400 WILSON BLVD
ARLINGTON, VA 22209
ATTN DIR, MATERIALS SCIENCES

DIRECTOR
DEFENSE INTELLIGENCE AGENCY
WASHINGTON, DC 20301
ATTN DTICI, ROBERT I. RUBENSTEIN
ATTN DB-4C, F. O'FARRELL
ATTN RDS-4B
ATTN RDS-3A, TECHNICAL LIBRARY

DIRECTOR
DEFENSE NUCLEAR AGENCY
WASHINGTON, DC 20305
ATTN STVL
ATTN TISI
ATTN TITL
ATTN RAEV

COMMANDER
FIELD COMMAND
DEFENSE NUCLEAR AGENCY
KIRTLAND AFB, NM 87115
ATTN FCPR

DIRECTOR
JOINT STRAT TGT PLANNING STAFF
OFFUTT AFB
OMAHA, NB 68113
ATTN JSAS

CHIEF
LIVERMORE DIVISION FLD COMMAND, DNA
LAWRENCE LIVERMORE LABORATORY
P.O. BOX 808
LIVERMORE, CA 94550
ATTN FCPR

UNDER SECY OF DEF FOR RSCH & ENGRG
DEPARTMENT OF DEFENSE
WASHINGTON, DC 20301
ATTN S&SS (OS)

COMMANDER
BMD SYSTEM COMMAND
P.O. BOX 1500
HUNTSVILLE, AL 35807
ATTN SSC-TEN

COMMANDER
BALLISTIC MISSILE DEFENSE ADVANCED
TECHNOLOGY CENTER
P.O. BOX 1500
HUNTSVILLE, AL 35807
ATTN ATC-D, LARRY HAVARD

DEP CHIEF OF STAFF FOR RSCH DEV & ACQ
DEPARTMENT OF THE ARMY
WASHINGTON, DC 20310
ATTN DAMA-CSM-N

DISTRIBUTION (Cont'd)

COMMANDER REDSTONE SCIENTIFIC INFORMATION CTR U.S. ARMY R & D COMMAND REDSTONE ARSENAL, AL 35809 ATTN CHIEF, DOCUMENTS	AF WEAPONS LABORATORY, AFSC KIRTLAND AFB, NM 87117 ATTN CA ATTN NT ATTN SUL ATTN DYP
COMMANDER US ARMY MISSILE R&D COMMAND REDSTONE ARSENAL, AL 35809 ATTN DRCPM-PE-EA	HQ USAF/RD WASHINGTON, DC 20330 ATTN RDQSM
COMMANDER US ARMY NUCLEAR & CHEMICAL AGENCY 7500 BACKLICK ROAD BUILDING 2073 SPRINGFIELD, VA 22150 ATTN LIBRARY	SAMSO/DY POST OFFICE BOX 92960 WORLDWAY POSTAL CENTER LOS ANGELES, CA 90009 (TECHNOLOGY) ATTN DYS
COMMANDER US ARMY TEST AND EVALUATION COMMAND ABERDEEN PROVING GROUND, MD 21005 ATTN DRSTE-EL	SAMSO/IN POST OFFICE BOX 92960 WORLDWAY POSTAL CENTER LOS ANGELES, CA 90009 (INTELLIGENCE) ATTN IND, MAJ DARRYL S. MUSKIN
CHIEF OF NAVAL OPERATIONS NAVY DEPARTMENT WASHINGTON, DC 20350 ATTN ROBERT A. BLAISE, 604C4	SAMSO/MN NORTON AFB, CA 92409 (MINUTEMAN) ATTN MNH
COMMANDER NAVAL ELECTRONIC SYSTEMS COMMAND NAVAL ELECTRONIC SYSTEMS CMD HQS WASHINGTON, DC 20360 ATTN CODE 5032	SAMSO/SK POST OFFICE BOX 92960 WORLDWAY POSTAL CENTER LOS ANGELES, CA 90009 (SPACE COMM SYSTEMS) ATTN SKF, PETER H. STADLER
COMMANDING OFFICER NAVAL INTELLIGENCE SUPPORT CTR 4301 SUITLAND ROAD, BLDG 5 WASHINGTON, DC 20390 ATTN NTSC-45	UNIVERSITY OF CALIFORNIA LAWRENCE LIVERMORE LABORATORY P.O. BOX 808 LIVERMORE, CA 94550 ATTN L-18 ATTN L-153 ATTN JOHN NUCKOLLS, A DIV L-545 ATTN TECH INFO DEPT, L-3
DIRECTOR NAVAL RESEARCH LABORATORY WASHINGTON, DC 20375 ATTN GERALD COOPERSTEIN, CODE 7770	SANDIA LABORATORIES P.O. BOX 5800 ALBUQUERQUE, NM 87115 ATTN DOC CON FOR 3141 SANDIA RPT COLL ATTN DOC CON FOR 5240 GERALD YONAS
OFFICER-IN-CHARGE NAVAL SURFACE WEAPONS CENTER WHITE OAK, SILVER SPRING, MD 20910 ATTN CODE WR43 ATTN CODE WA501, NAVY NUC PRGMS OFF ATTN CODE F34, R. A. SMITH	AVCO RESEARCH & SYSTEMS GROUP 201 LOWELL STREET WILMINGTON, MA 01887 ATTN RESEARCH LIB, A830, RM 7201
COMMANDER NAVAL SURFACE WEAPONS CENTER DAHLGREN, VA 22448	BDM CORP 7915 JONES BRANCH DRIVE MCLEAN, VA 22101 ATTN TECHNICAL LIBRARY
COMMANDER NAVAL WEAPONS CENTER CHINA LAKE, CA 93555 ATTN CODE 533, TECH LIB	

DISTRIBUTION (Cont'd)

BOEING CO.
P.O. BOX 3707
SEATTLE, WA 98124
ATTN AEROSPACE LIBRARY

DIKEWOOD INDUSTRIES, INC.
1009 BRADBURY DRIVE, S.E.
ALBUQUERQUE, NM 87106
ATTN L. DAVIS

EG&G WASHINGTON ANALYTICAL
SERVICES CENTER, INC.
P.O. BOX 10218
ALBUQUERQUE, NM 87114
ATTN TECHNICAL LIBRARY

FORD AEROSPACE & COMMUNICATIONS CORP
FORD & JAMBOREE ROADS
NEWPORT BEACH, CA 92663
ATTN TECH INFO SECTION

FORD AEROSPACE & COMMUNICATIONS CORP
3939 FABIAN WAY
PALO ALTO, CA 94303
ATTN LIBRARY

GENERAL ELECTRIC CO.
SPACE DIVISION
VALLEY FORGE SPACE CENTER
P.O. BOX 8555
PHILADELPHIA, PA 19101
ATTN J. PEDEN VFSC, 4230M

GENERAL ELECTRIC CO.-TEMPO
CENTER FOR ADVANCED STUDIES
816 STATE STREET (P.O. DRAWER QO)
SANTA BARBARA, CA 93102
ATTN DASIA C

INSTITUTE FOR DEFENSE ANALYSES
400 ARMY-NAVY DRIVE
ARLINGTON, VA 22202
ATTN IDA LIBRARIAN R. SMITH

ION PHYSICS CORP
SOUTH BEDFORD STREET
BURLINGTON, MA 01803
ATTN H. MILDE

IRT CORP.
P.O. BOX 81087
SAN DIEGO, CA 92138
ATTN R. MERTZ

JAYCOR
1401 CAMINO DEL MAR
DEL MAR, CA 92014
ATTN E. WENAAS

JAYCOR
205 WHITING STREET, SUITE 500
ALEXANDRIA, VA 22304
ATTN R. SULLIVAN

KAMAN SCIENCES CORP.
P.O. BOX 7463
COLORADO SPRINGS, CO 80933
ATTN A. BRIDGES
ATTN J. HOFFMAN
ATTN D. BRYCE
ATTN W. WARE

LOCKHEED MISSILES AND SPACE CO., INC.
3251 HANOVER STREET
PALO ALTO, CA 94304
ATTN LLOYD F. CHASE

MAXWELL LABORATORIES, INC.
9244 BALBOA AVENUE
SAN DIEGO, CA 92123
ATTN A. RICHARD MILLER
ATTN PETER KORN
ATTN ALAN C. KOLB

MCDONNELL DOUGLAS CORP.
5301 BOLSA AVENUE
HUNTINGTON BEACH, CA 92647
ATTN STANLEY SCHNEIDER

MISSION RESEARCH CORP.
735 STATE STREET
SANTA BARBARA, CA 93101
ATTN WILLIAM C. HART
ATTN C. LONGMIRE

MISSION RESEARCH CORP.-SAN DIEGO
P.O. BOX 1209
LA JOLLA, CA 92038
(VICTOR A. J. VAN LINT)
ATTN V. A. J. VAN LINT

NORTHROP CORP.
NORTHROP RESEARCH AND TECHNOLOGY CTR
ONE RESEARCH PARK
PALOS VERDES PENN, CA 90274
ATTN LIBRARY

NORTHROP CORP.
ELECTRONIC DIVISION
2301 WEST 120TH STREET
HAWTHORNE, CA 90250
ATTN VINCENT R. DEMARTINO

PHYSICS INTERNATIONAL CO.
2700 MERCED STREET
SAN LEANDRO, CA 94577
ATTN DOC CON FOR BERNARD H. BERNSTEIN
ATTN DOC CON FOR GEORGE FRAZIER
ATTN DOC CON FOR PHILIP W. SPENCE
ATTN DOC CON FOR SIDNEY D. PUTNAM

DISTRIBUTION (Cont'd)

PULSAR ASSOCIATES, INC.
11491 SORRENTO VALLEY BLVD
SAN DIEGO, CA 92121
ATTN CARLETON H. JONES, JR.

R & D ASSOCIATES
P.O. BOX 9695
MARINA DEL REY, CA 90291
ATTN C. MACDONALD
ATTN W. GRAHAM, JR.
ATTN LEONARD SCHLESSINGER

SCIENCE APPLICATIONS, INC.
P.O. BOX 2351
LA JOLLA, CA 92038
ATTN J. ROBERT BEYSTER

SPIRE CORP.
P.O. BOX D
BEDFORD, MA 01730
ATTN ROGER G. LITTLE

SRI INTERNATIONAL
333 RAVENSWOOD AVENUE
MENLO PARK, CA 94025
ATTN SETSUO DDAIRIKI

SYSTEMS, SCIENCE & SOFTWARE, INC.
P.O. BOX 1620
LA JOLLA, CA 92038
ATTN ANDREW R. WILSON

TEXAS TECH UNIVERSITY
P.O. BOX 5404 NORTH COLLEGE STATION
LUBBOCK, TX 79417
ATTN TRAVIS L. SIMPSON

TRW DEFENSE & SPACE SYS GROUP
ONE SPACE PARK
REDONDO BEACH, CA 90278
ATTN TECH INFO CENTER/S-1930

VOUGHT CORP.
MICHIGAN DIVISION
38111 VAN DYKE ROAD
STERLING HEIGHTS, MI 48077
ATTN TECH LIB

US ARMY ELECTRONICS RESEARCH
& DEVELOPMENT COMMAND
ATTN WISEMAN, ROBERT S., DR., DRDEL-CT
ATTN PAO

HARRY DIAMOND LABORATORIES
ATTN 00100, COMMANDER/TECHNICAL DIR/TSO

ATTN CHIEF, 00210

ATTN CHIEF, DIV 10000

ATTN CHIEF, DIV 20000

ATTN CHIEF, DIV 30000

ATTN CHIEF, DIV 40000

ATTN CHIEF, LAB 11000

ATTN CHIEF, LAB 13000

ATTN CHIEF, LAB 15000

ATTN CHIEF, LAB 22000

ATTN CHIEF, LAB 21000

ATTN CHIEF, LAB 34000

ATTN CHIEF, LAB 36000

ATTN CHIEF, LAB 47000

ATTN CHIEF, LAB 48000

ATTN RECORD COPY, 94100

ATTN HDL LIBRARY, 41000 (5 COPIES)

ATTN HDL LIBRARY, 41000 (WOODBRIDGE)

ATTN CHAIRMAN, EDITORIAL COMMITTEE

ATTN TECHNICAL REPORTS BRANCH, 41300

ATTN LEGAL OFFICE, 97000

ATTN LANHAM, C., 00210

ATTN WILLIS, B., 47400

ATTN CHIEF, 22100

ATTN CHIEF, 22300

ATTN CHIEF, 22800

ATTN CHIEF, 22900

ATTN CHIEF, 21100

ATTN CHIEF, 21200

ATTN CHIEF, 21300

ATTN CHIEF, 21400

ATTN CHIEF, 21500

ATTN HUTTLIN, G. A., (15 COPIES)

ATTN STEWART, A. G., (15 COPIES)